L-426

RB No. 4C13

NATIONAL ADVISORY COMMITTEE FOR AERONAUTICS

WARTIME REPORT

ORIGINALLY ISSUED
March 1944 as
Restricted Bulletin 4C13

SOME EFFECTS OF PROPELLER OPERATION ON THE DISTRIBUTION OF THE LOAD ON THE VERTICAL TAIL SURFACE OF A TYPICAL PURSUIT AIRPLANE

By Harold H. Sweberg and Richard C. Dingeldein

Langley Memorial Aeronautical Laboratory
Langley Field, Va.

NACA

WASHINGTON

NATIONAL ADVISORY COMMITTEE FOR AERONAUTICS

RESTRICTED BULLETIN

L-426

SOME EFFECTS OF PROPELLER OPERATION ON THE DISTRIBUTION OF THE LOAD ON THE VERTICAL TAIL SURFACE OF A TYPICAL PURSUIT AIRPLANE

By Harold H. Sweberg and Richard C. Dingeldein

INTRODUCTION

The pressure distribution had been measured at several longitudinal sections of the vertical tail surface of the Curtiss P-40K airplane in the NACA full-scale tunnel. The tests were made for various angles of attack and angles of yaw with the propeller removed and with the propeller operating. These tests were incidental to a similar investigation of the horizontal-tail loading, the results of which are reported in reference 1.

The data are intended primarily to show the distribution of normal-force coefficient along the span of the vertical tail surface under conditions simulating flight. Some analysis has been made of the effects of propeller operation on the distribution of the load on the vertical tail surface.

SYMBOLS

C_L airplane lift coefficient

C_{N_t} vertical-tail normal-force coefficient $(N_t/q_o S_t)$

c_{n_t} vertical-tail section normal-force coefficient $(n_t/q_o c_t)$

Q_c torque coefficient $(Q/\rho V^2 D^3)$

T_c thrust coefficient $\left(\frac{\text{effective thrust}}{\rho V^2 D^2}\right)$.

N_t	vertical-tail normal force
n_t	vertical-tail section normal force
Q	propeller torque
Δp	difference in local static pressure between right and left surfaces of vertical tail
q_o	free-stream dynamic pressure
V	velocity
ρ	density of air
n	propeller rotational speed
S_t	area of vertical tail surface
D	propeller diameter
c_t	chord of vertical tail
α_T	angle of attack of thrust axis relative to free-stream direction, degrees
ψ	angle of yaw, degrees; positive when left wing moves forward
β	propeller blade angle measured at 0.75 radius, degrees
V/nD	propeller advance-diameter ratio
i_t	angle of stabilizer setting with respect to thrust axis; positive with trailing edge down

APPARATUS AND TESTS

The tests were conducted on the Curtiss P-40K airplane, which is a low-wing pursuit airplane weighing 7740 pounds and equipped with a V-1710-F4R Allison engine rated at 1000 horsepower at an altitude of 10,800 feet. A three-view drawing noting the principal dimensions of the airplane is presented in figure 1, and a photograph of the airplane mounted in the NACA full-scale tunnel is given as figure 2.

Four rows of flush-type static-pressure orifices were used to obtain the pressure distribution over the vertical tail surface. The location of the orifices is shown in figure 3. Inasmuch as there were no pressure orifices located very near the leading edge, a method similar to that described in reference 1 was used to obtain the leading-edge pressure peaks.

A summary of the complete test program is given in table I. Most of the tests were made with the propeller operating under conditions simulating rated power for an altitude of 10,000 feet. The remainder of the tests were made with the propeller removed and with the propeller operating at other thrust and torque coefficients in order that the effects of propeller operation on the tail load distribution might be determined. The range of angle of yaw for these tests was $\pm 10^{\circ}$. A few force tests were also made to determine the variation of lift coefficient with angle of attack of the airplane with the propeller removed and operating. The tunnel airspeed for all the tests was 85 miles per hour.

A constant propeller-blade-angle setting of 35° measured at the 0.75 radius was used throughout the tunnel tests. It was desired for the tests to reproduce the torque coefficients obtained in flight and to simulate the thrust coefficients as nearly as possible, inasmuch as the slipstream rotation was considered to have more effect on the vertical-tail loading than the increase in local velocity due to the thrust of the propeller. With the blade angle at 35°, it was possible to reproduce the torque coefficients of the constant-speed propeller and to simulate very nearly the thrust coefficients. Figure 4 shows the variation of blade angle and V/nD with lift coefficient, and figure 5 shows the variation of Q_c and T_c with lift coefficient for the constant-speed propeller (flight condition) and for the propeller operating at constant blade angle. The variation of lift coefficient with angle of attack of the airplane with the propeller removed and with the propeller operating at rated power at an altitude of 10,000 feet is shown in figure 6.

RESULTS AND DISCUSSION

A few typical chordwise pressure distributions over the vertical tail surface of the P-40K airplane are

shown in figures 7 to 10 for a lift coefficient of 0.820. The pressure distributions are given for four angles of yaw ($\psi = 0^\circ$, 5°, 10°, and -10°) with the propeller torque coefficients varied from 0 to 0.036. The effects of propeller operation alone on the chordwise pressure distribution are shown directly in figure 7, in which $\psi = 0^\circ$. The leading edge of the fin was set $1\frac{1}{2}^\circ$ to the left for these tests, so that the resultant load was negative (load to the left) for the propeller-removed condition. Propeller operation caused changes in the load on the vertical tail in a positive direction (load to the right). The changes in the pressure distributions that were measured over the upper two rows of the vertical tail were approximately proportional to the changes in torque coefficient; the changes in the pressure distributions over the lower two rows, however, were small and not consistent with the changes in torque coefficient, probably because of the presence of the fuselage boundary-layer flow.

The chordwise pressure-distribution measurements have been integrated to obtain the variation of section normal-force coefficient along the vertical-tail span. The results of these integrations at three lift coefficients for the airplane with propeller removed are shown in figure 11. As the angle of yaw was varied from 0° to 10°, the section normal-force coefficients measured on the lower row, which was blanketed by the fuselage, changed only slightly. The lower portion of the rudder will therefore be ineffective in producing a stabilizing yawing moment as the airplane is yawed from its neutral position. The maximum change in section normal-force coefficient occurred along the row located about halfway between the elevator hinge line and the top of the fin. Similar normal-force distributions have been measured over the vertical tail of the P-47B airplane (reference 2).

The effects of propeller operation on the spanwise distribution of normal-force coefficient on the vertical tail surface are shown in figures 12 to 15 for four angles of yaw ($\psi = 0^\circ$, 5°, 10°, and -10°). For purposes of comparison, the corresponding distributions for the airplane with the propeller removed are included. Propeller operation produced an increment of load on the vertical tail to the right, regardless of the direction of yaw (compare figs. 14 and 15); this increment therefore resulted from changes in the local angles of attack

of the vertical tail that were due to the slipstream rotation. The effects of increases in the local velocity at the tail due to increases in the thrust coefficient appear to be of lesser importance. The largest effects of propeller operation were measured at the upper two stations and were most pronounced at the highest angles of yaw ($\psi = \pm 10°$). Under these conditions, there is a large concentration of the vertical-tail load in a small region centering about the middle of the fin (figs. 14 and 15).

Computations of the total normal-force coefficients on the vertical tail have been made from the results of the span load distributions. A summary of these computations is presented in the last column of table I for all the test conditions. The variation of vertical-tail normal-force coefficient with angle of attack of the airplane when the propeller was removed is shown in figure 16 for three angles of yaw. For the propeller-removed condition, the vertical-tail normal-force coefficient decreased slightly with increased angle of attack, probably because of the upward displacement of the wing and fuselage wakes with increasing angle of attack.

The effect of propeller operation on the variation of vertical-tail normal-force coefficient with angle of yaw is shown in figure 17 for a lift coefficient of 0.294 and in figure 18 for a lift coefficient of 0.820. The most notable effect shown in these figures is that, for the range of propeller operating conditions used in these tests, the slopes of the curves of C_{N_t} against ψ changed only slightly with increased power; however, at any particular angle of yaw the normal-force coefficient increased positively as the power was increased.

The data of figures 17 and 18 have been cross-plotted in figure 19 to show the effects of slipstream rotation on the vertical-tail normal-force coefficients. The effects of increasing the thrust coefficient are also included inasmuch as the thrust and the torque were varied together. These results further bring out the point that, regardless of the direction of the initial load on the tail, propeller operation always resulted in an increment of tail load in a positive direction. As expected, the increase was largest for $\psi = 10°$ because for this angle of yaw both the thrust and the torque

tended to increase the load in a positive direction. For negative angles of yaw the increase in axial velocity due to the propeller thrust will tend to increase the force on the tail in the direction of the initial load (negative), but the slipstream rotation due to the propeller torque will tend to increase the load in a positive direction for right-hand propeller operation. For the range of propeller-operating conditions simulated in these tests (rated power at an altitude of 10,000 ft), the effects of increases in torque coefficient are predominant.

SUMMARY OF RESULTS

The results of measurements made in the NACA full-scale tunnel on a typical pursuit airplane to determine the effects of propeller operation on the vertical-tail load distribution showed the following:

1. Propeller operation caused an increment of force on the vertical tail in a positive direction (force to right) regardless of the direction of the initial load on the surface.

2. The largest effects of propeller operation were measured at a section located approximately in the middle of the fin and resulted in a large concentration of the vertical-tail load at this section.

3. The distribution of the load over the portion of the vertical tail that is blanketed by the fuselage changed only slightly with changes in either yaw angle or propeller operation.

4. For the range of propeller-operating conditions of these tests, the slopes of the curves of vertical-tail normal-force coefficient against angle of yaw varied only slightly with increase in thrust and torque coefficients.

5. The effects of increases in slipstream rotation resulting from increases in propeller torque on the vertical-tail loading were far more pronounced than the effects of increases in the axial velocity in the slipstream due to increases in propeller thrust.

Langley Memorial Aeronautical Laboratory,
National Advisory Committee for Aeronautics,
Langley Field, Va.

REFERENCES

1. Sweberg, Harold H., and Dingeldein, Richard C.: Effects of Propeller Operation and Angle of Yaw on the Distribution of the Load on the Horizontal Tail Surface of a Typical Pursuit Airplane. NACA ARR No. 4B10, Feb. 1944.

2. Dingeldein, Richard C.: Full-Scale Tunnel Investigation of the Pressure Distribution over the Tail of the P-47B Airplane. NACA ARR No. 3E25, May 1943.

Table I.- Summary of Tests and Results

Run	C_L	α_T, deg	ψ, deg	V/nD	C_{N_α}
1	0.066	-1.1	0	—	-0.049
2	.294	1.9	0	—	- .054
3	.820	8.7	0	—	- .066
4	.066	-1.1	5	—	.052
5	.294	1.9	5	—	.059
6	.820	8.7	5	—	.041
7	.066	-1.1	10	—	.213
8	.294	1.9	10	—	.207
9	.820	8.7	10	—	.183
10	.066	-1.1	0	1.70	-.043
11	.150	-0.3	0	1.56	-.040
12	.294	1.6	0	1.37	-.042
13	.294	1.6	0	1.56	-.046
15	.294	1.7	0	1.70	-.031
17	.820	7.4	0	.99	.028
18	.820	7.8	0	1.37	-.049
21	.820	8.2	0	1.65	-.047
23	.066	-1.1	5	1.70	.072
24	.150	-0.3	5	1.56	.080
25	.294	1.6	5	1.37	.097
26	.294	1.6	5	1.56	.073
28	.294	1.7	5	1.70	.069
30	.820	7.4	5	.99	.119
31	.820	7.8	5	1.37	.079
33	.820	8.2	5	1.65	.055
35	.066	-1.1	10	1.70	.263
36	.150	-0.3	10	1.56	.271
37	.294	1.6	10	1.37	.281
38	.294	1.6	10	1.56	.276
40	.294	1.7	10	1.70	.245
42	.820	7.4	10	.99	.345
43	.820	7.8	10	1.37	.265
45	.820	8.2	10	1.65	.224
47	.066	-1.1	-10	1.70	-.360
48	.150	-0.3	-10	1.56	-.353
49	.294	1.6	-10	1.37	-.303
50	.294	1.6	-10	1.56	-.336
51	.294	1.7	-10	1.70	-.322
52	.820	7.4	-10	.99	-.225
53	.820	7.8	-10	1.37	-.259
54	.820	8.2	-10	1.65	-.292

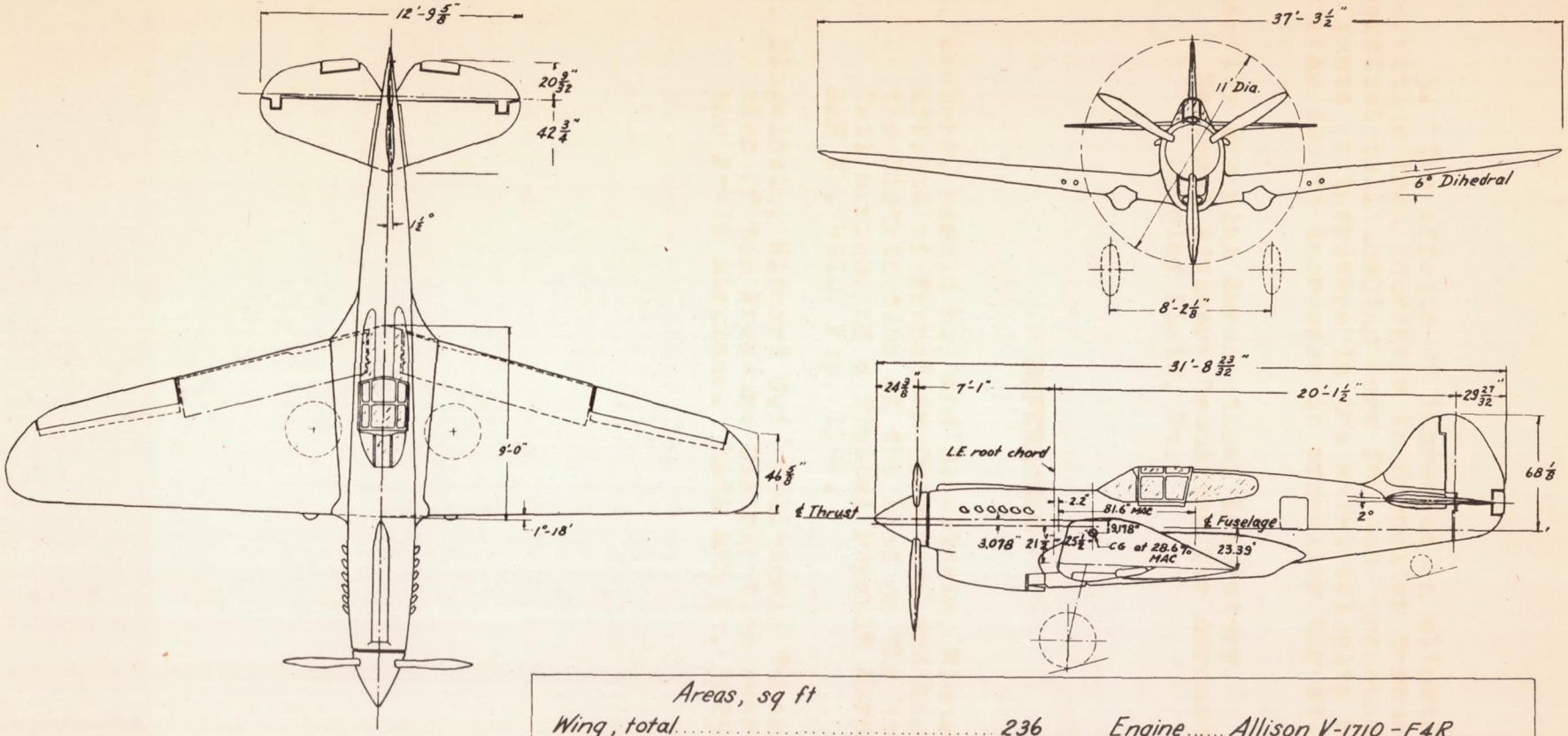

Areas, sq ft			
Wing, total	236	Engine	Allison V-1710-F4R
Stabilizer (incl. 3.56 sq ft of fuselage)	30.86	BHP normal rating - 1000 at 2600 rpm at 10,800 ft	
Elevator (incl. 3.8 sq ft balance, 1.68 sq ft tab)	17.44	Propeller gear ratio	2:1
Fin	9.18	Gross weight, design	7740 lb
Rudder (incl. 1.94 sq ft balance, 0.55 sq ft tab)	13.74		

Figure 1.- Three-view drawing of the P-40K airplane.

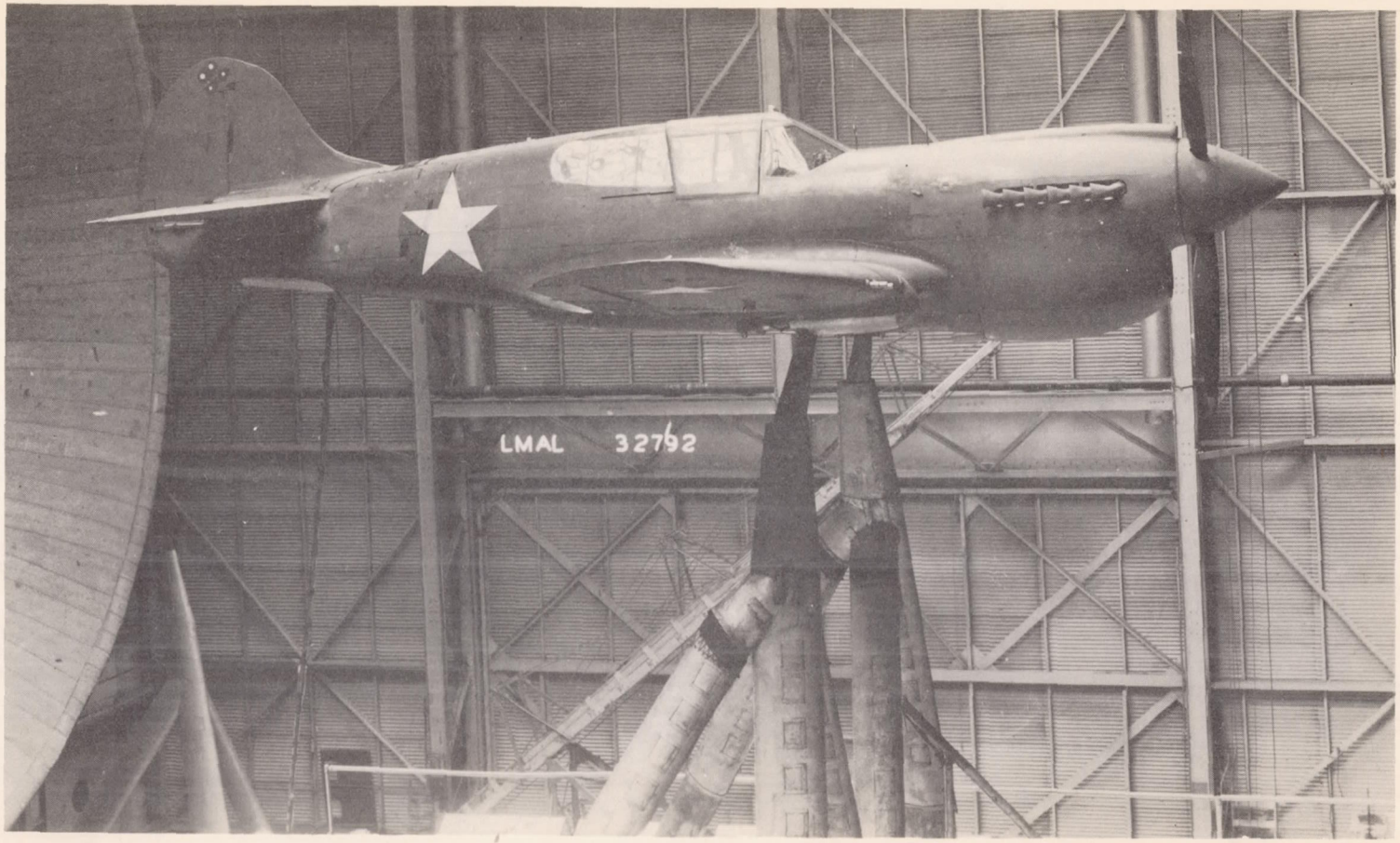

Figure 2.- The P-40K airplane mounted in the NACA full-scale tunnel.

L-926

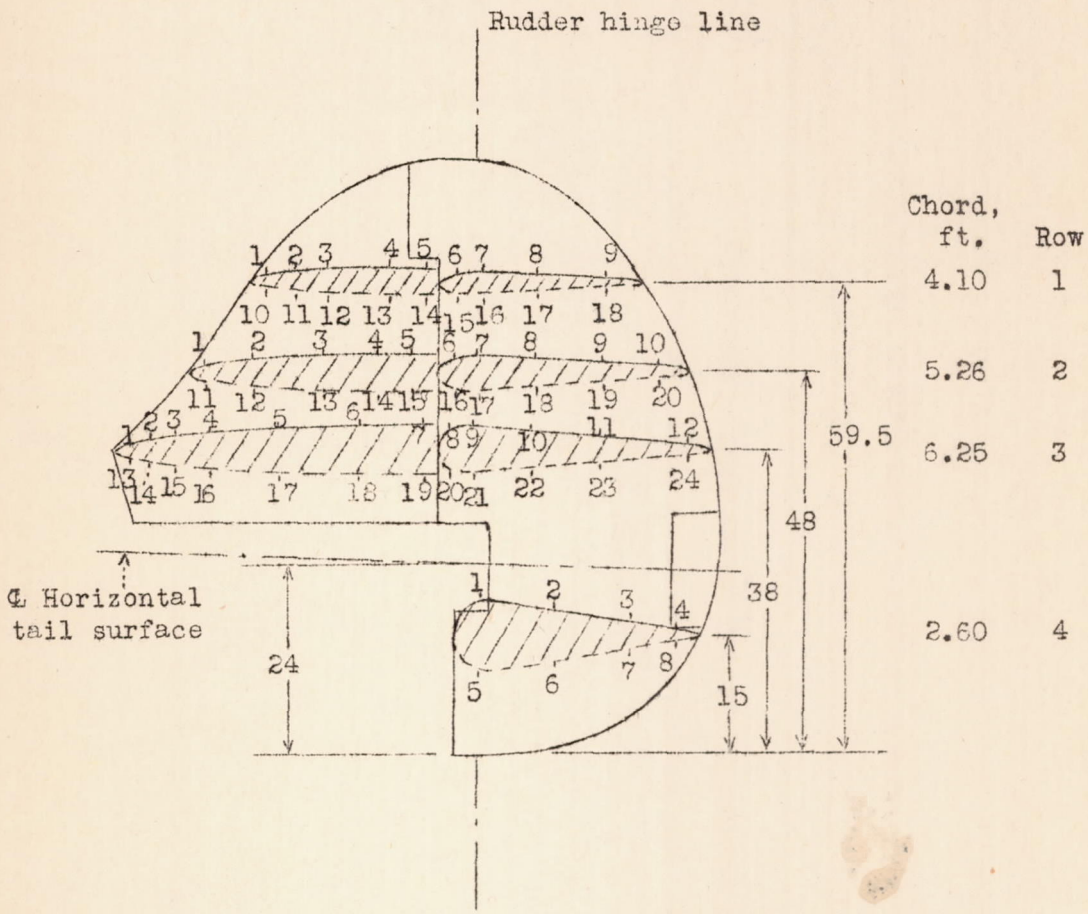

Figure 3.- Location and identification of vertical-tail-surface orifices.

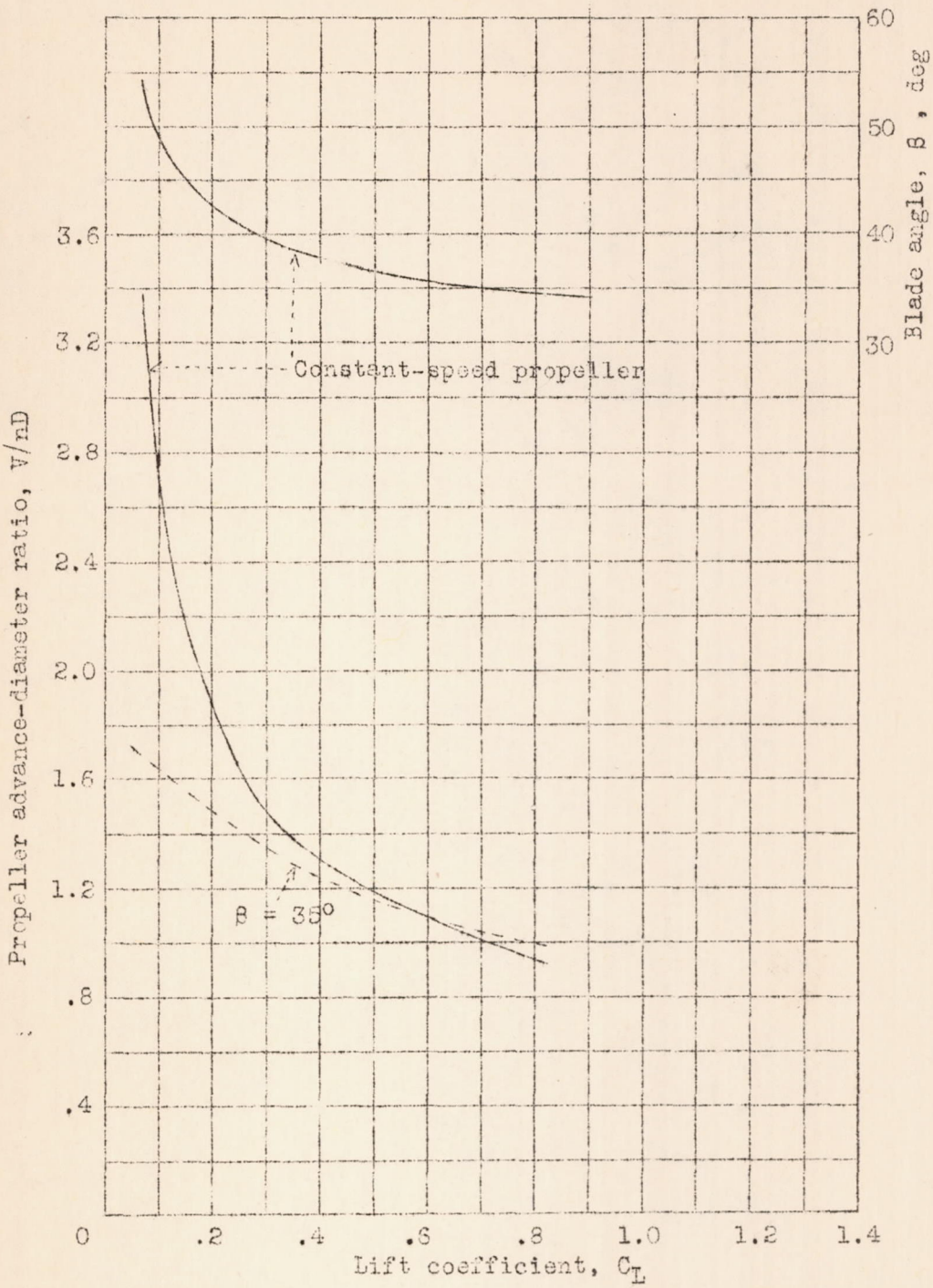

Figure 4.- Variation of β and V/nD with C_L for the constant-speed propeller and the propeller operating at constant blade angle. Rated power at 10,000 feet altitude.

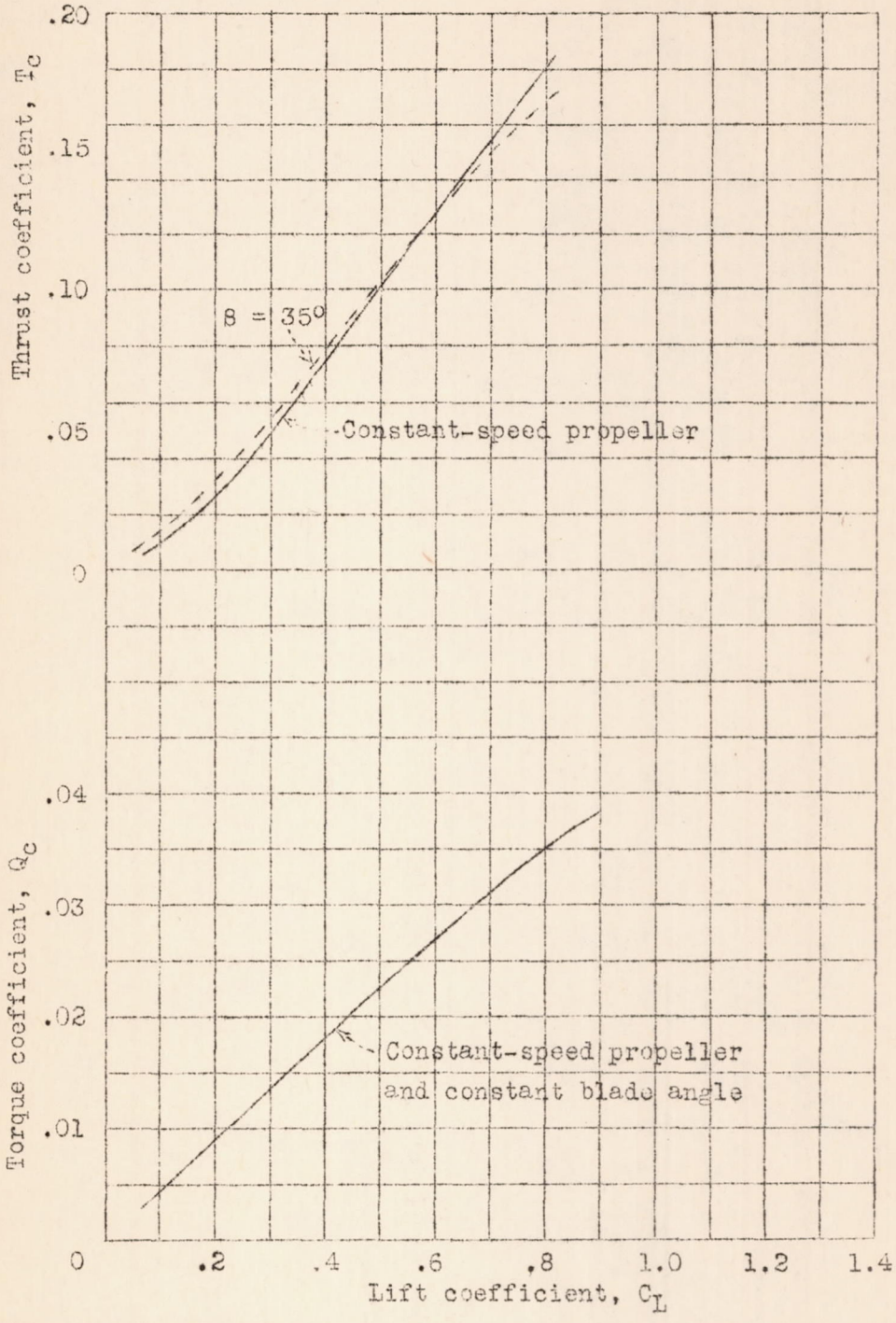

Figure 5.- Variation of T_c and Q_c with C_L for the constant-speed propeller and the propeller operating at constant blade angle. Rated power at 10,000 feet altitude.

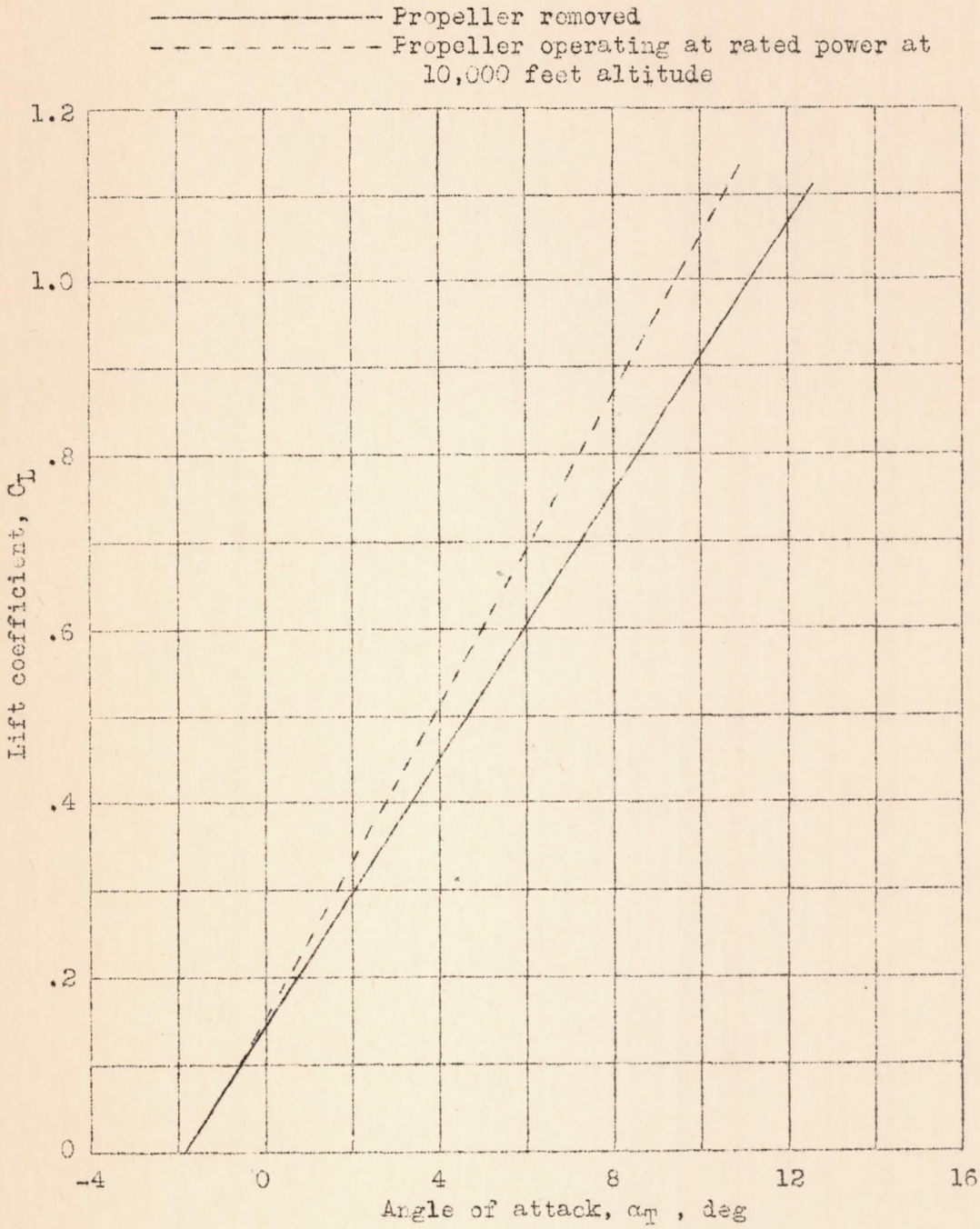

Figure 6.- Lift curves for the P-40K airplane with the propeller removed and operating at rated power at 10,000 feet altitude. Flaps retracted; i_t , 2.0°.

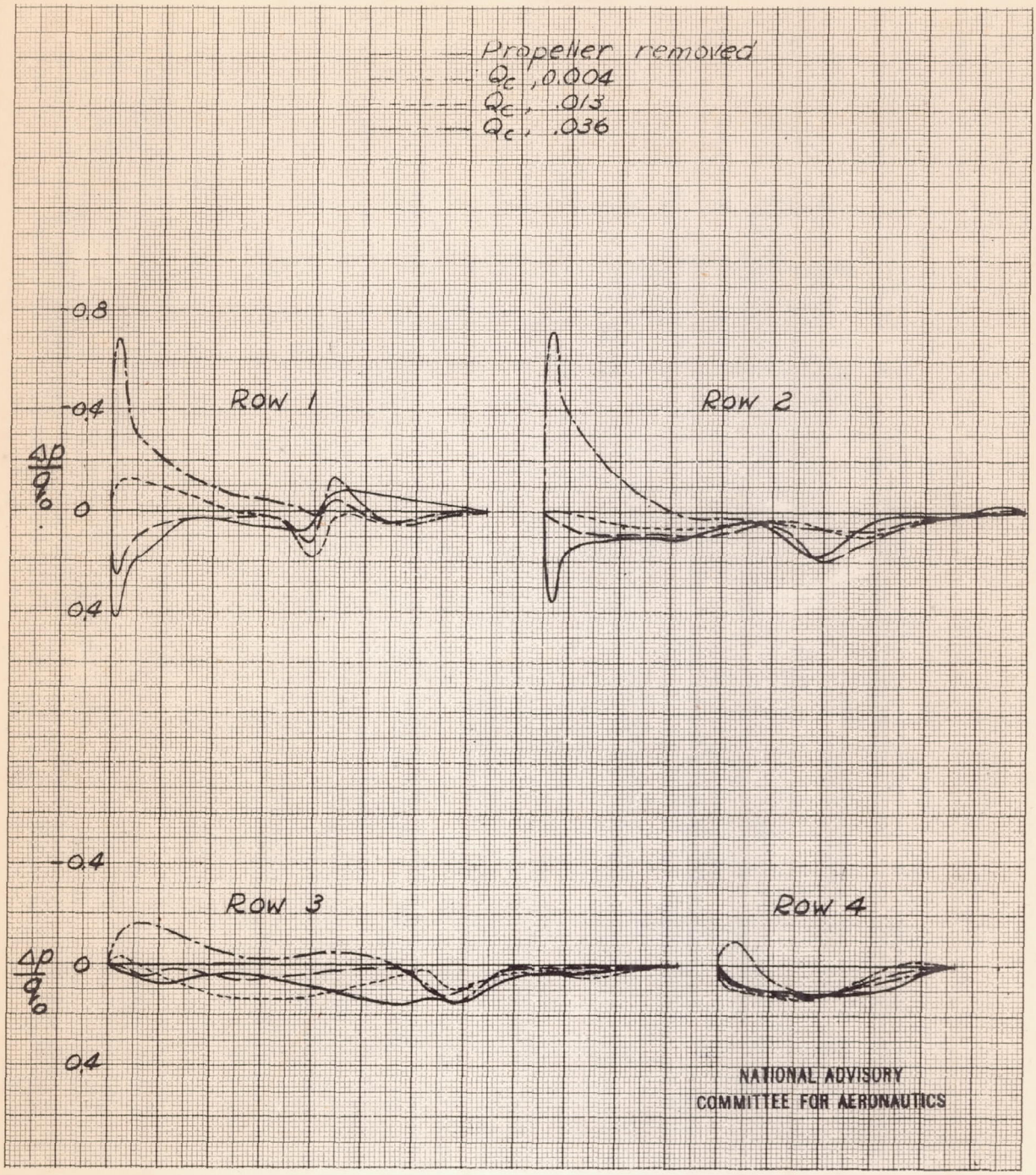

Figure 7.- Pressure distribution at four sections of the vertical tail of the P-40K airplane. C_L , 0.820; ψ , 0°.

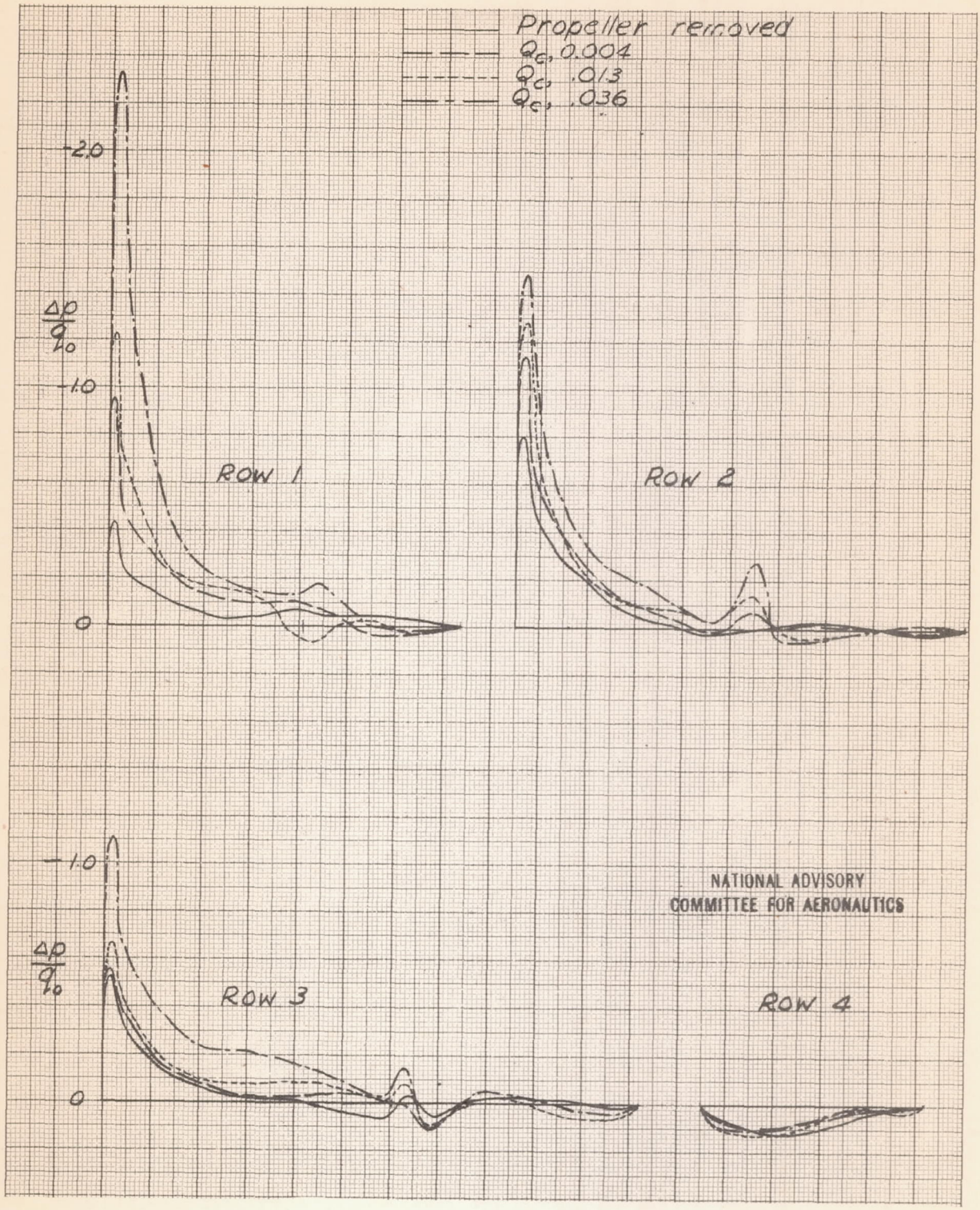

Figure 8.- Pressure distribution at four sections of the vertical tail of the P-40K airplane. C_L ,0.820; ψ , 5°.

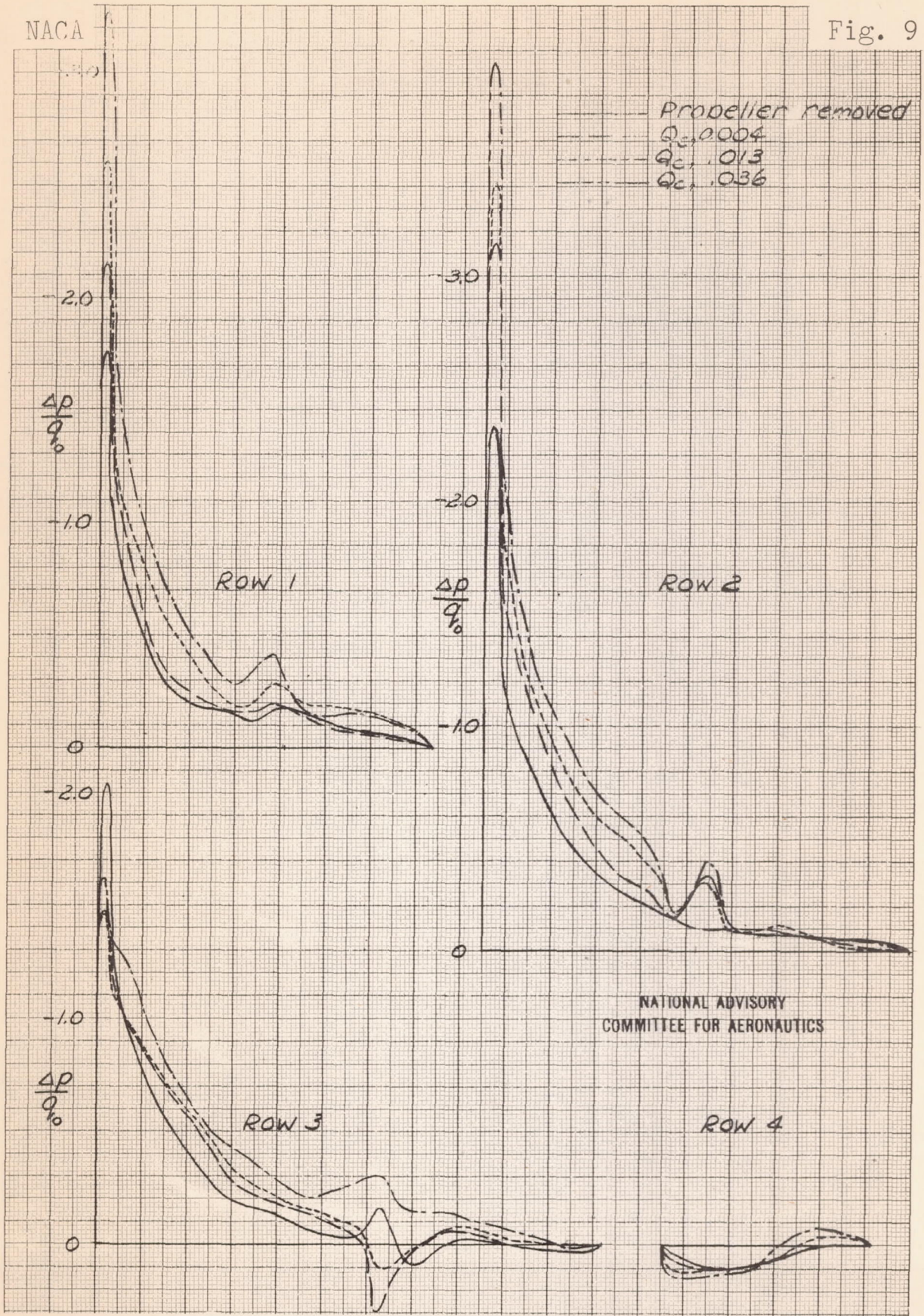

Figure 9.- Pressure distributions at four sections of the vertical tail of the P-40K airplane. C_L , 0.820; ψ ,10°.

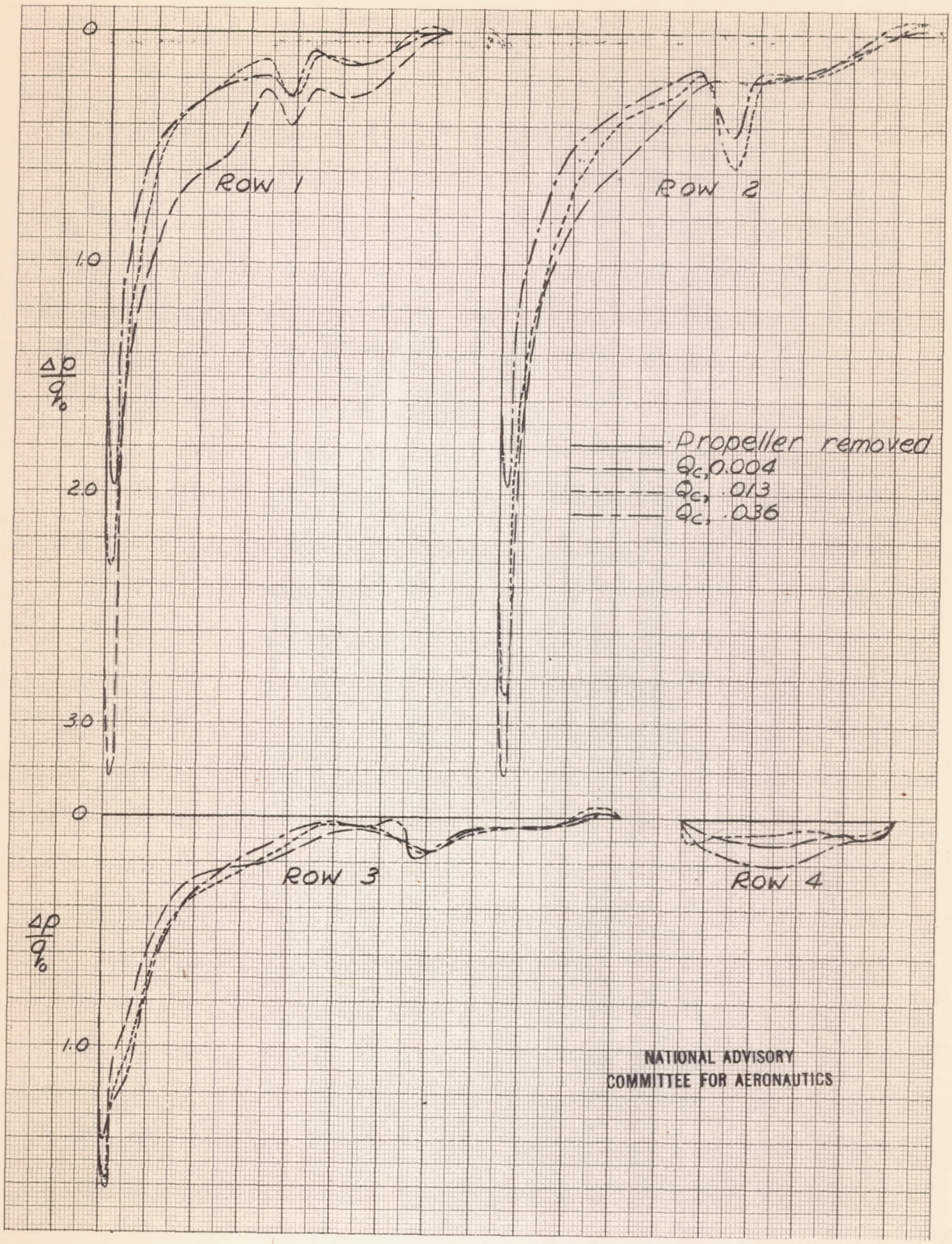

Figure 10.- Pressure distribution at four sections of the vertical tail of the P-40K airplane. C_L , 0.820; Ψ , -10°.

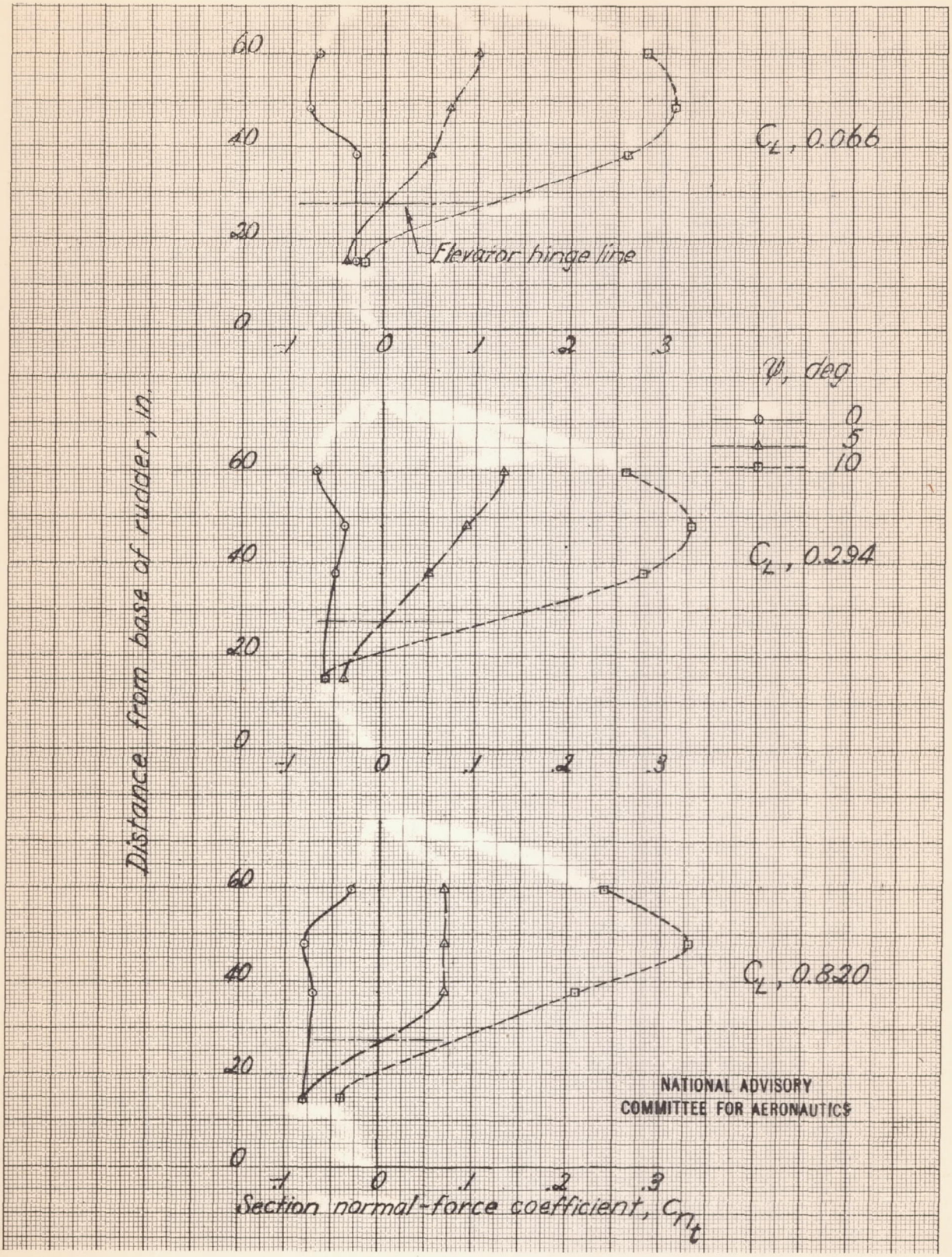

Figure 11.- Spanwise distribution of normal-force coefficient on vertical tail surface. Propeller removed.

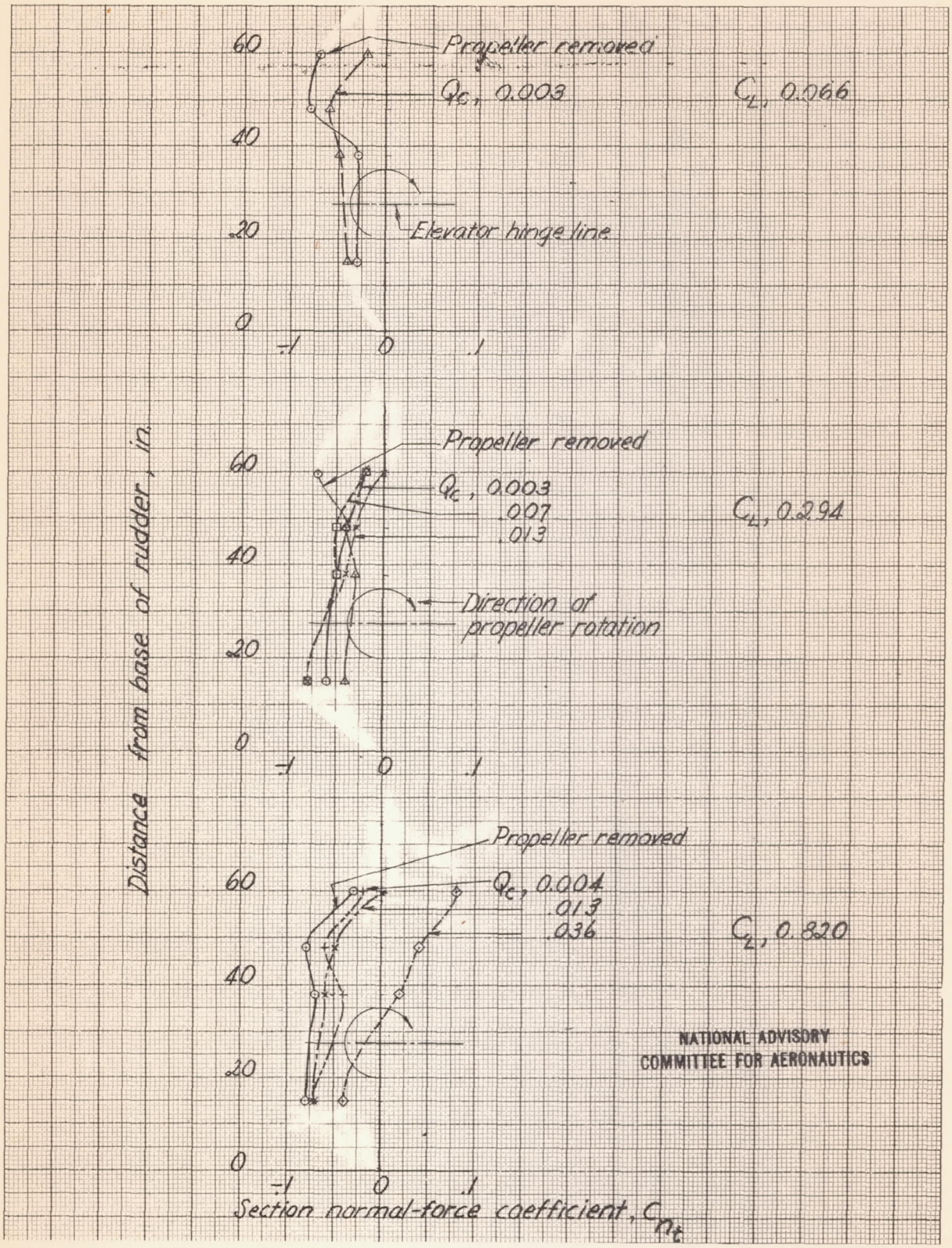

Figure 12.- Spanwise distribution of normal-force coefficient on vertical tail surface. ψ , 0°.

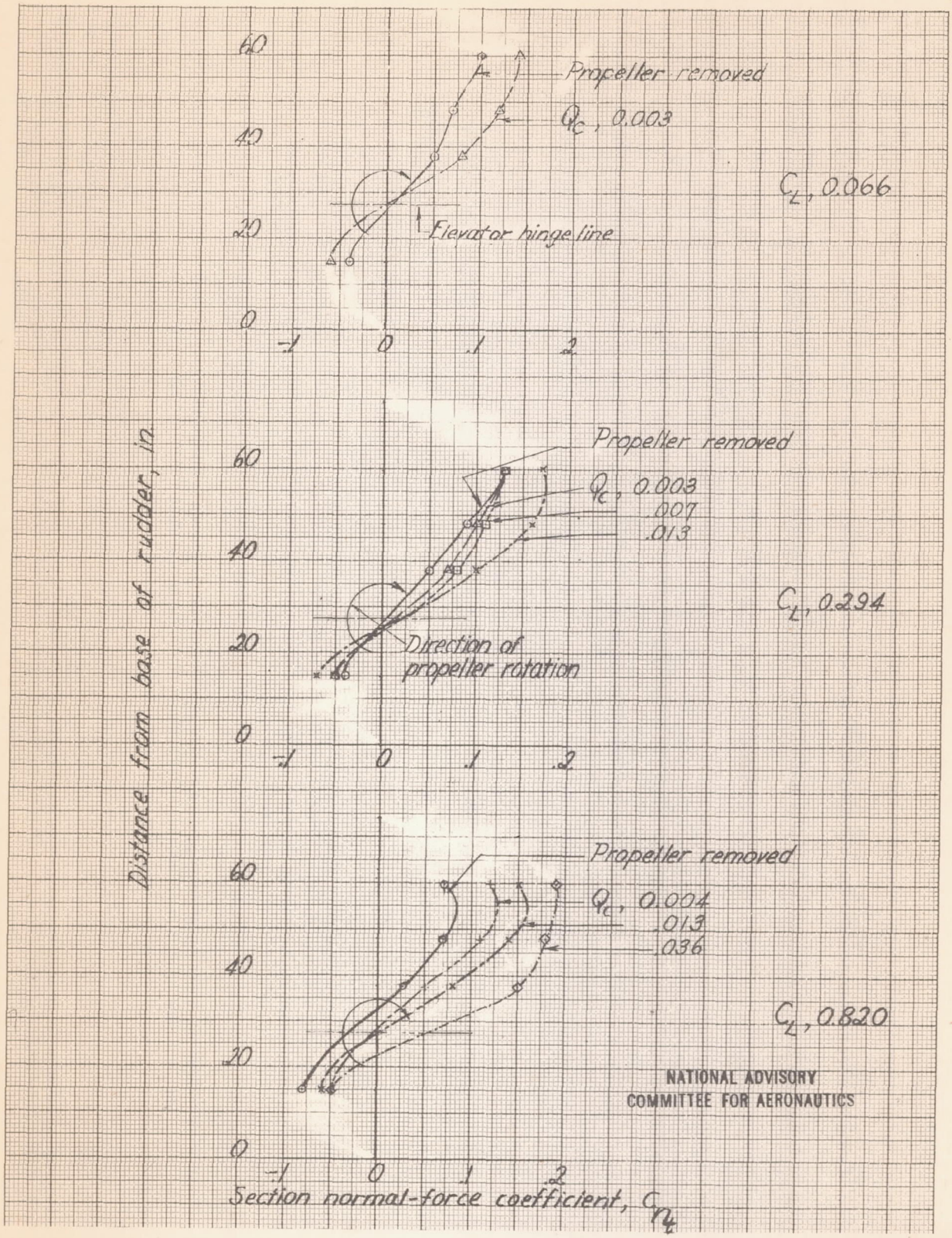

Figure 13.- Spanwise distribution of normal-force coefficient on vertical tail surface. ψ , 5°.

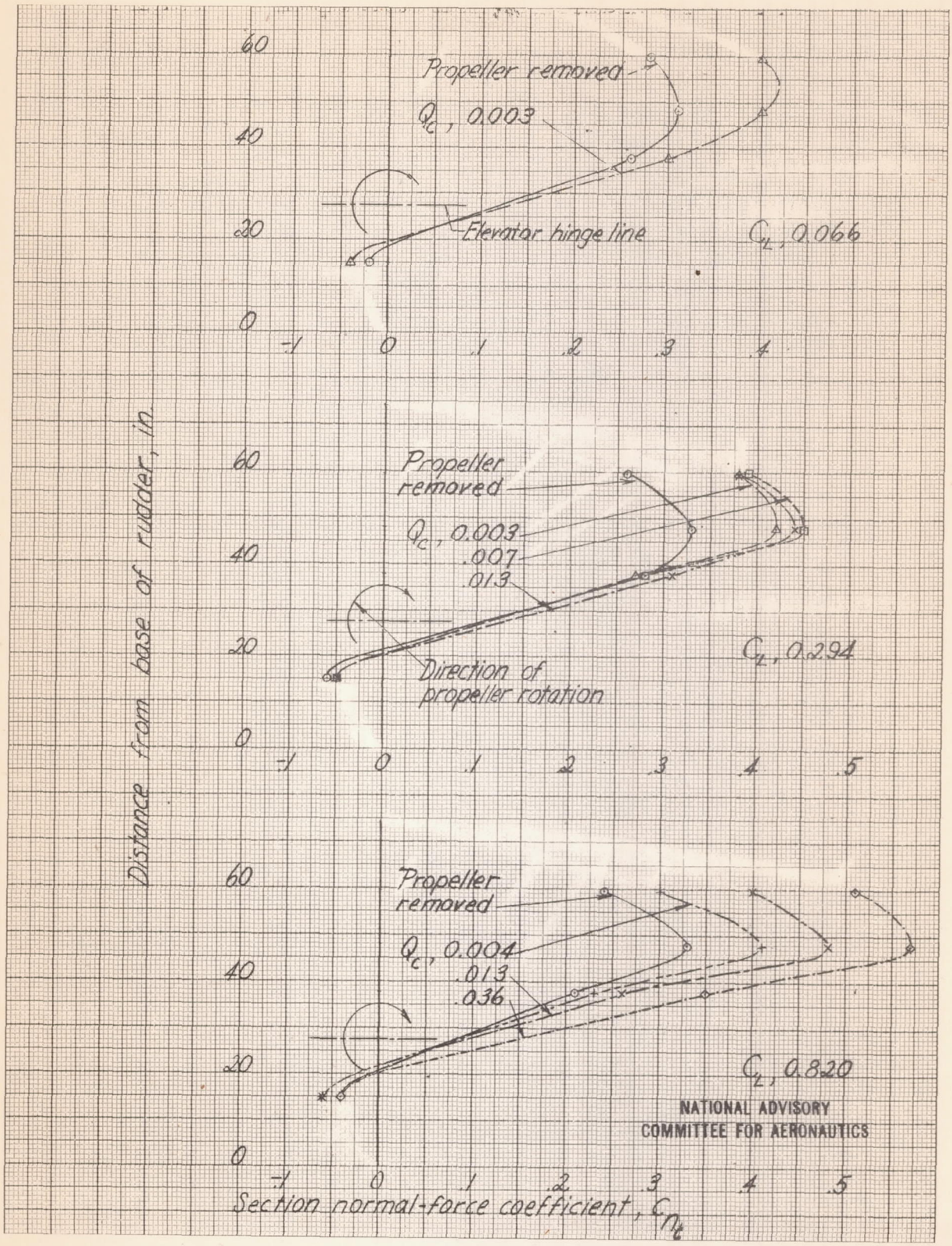

Figure 14.- Spanwise distribution of normal-force coefficient on vertical tail surface. ψ , 10°.

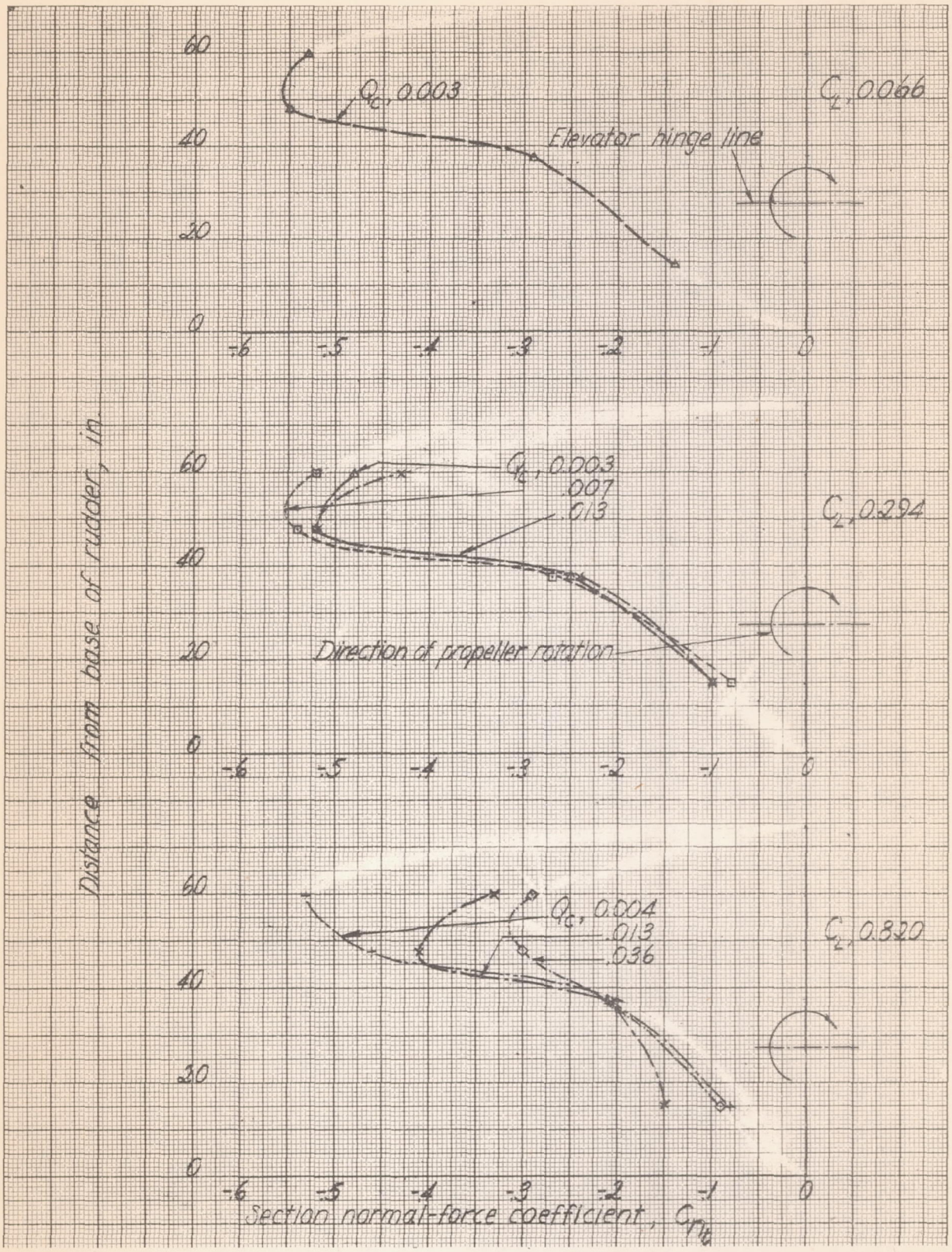

Figure 15.- Spanwise distribution of normal-force coefficient on vertical tail surface. ψ , -10°.

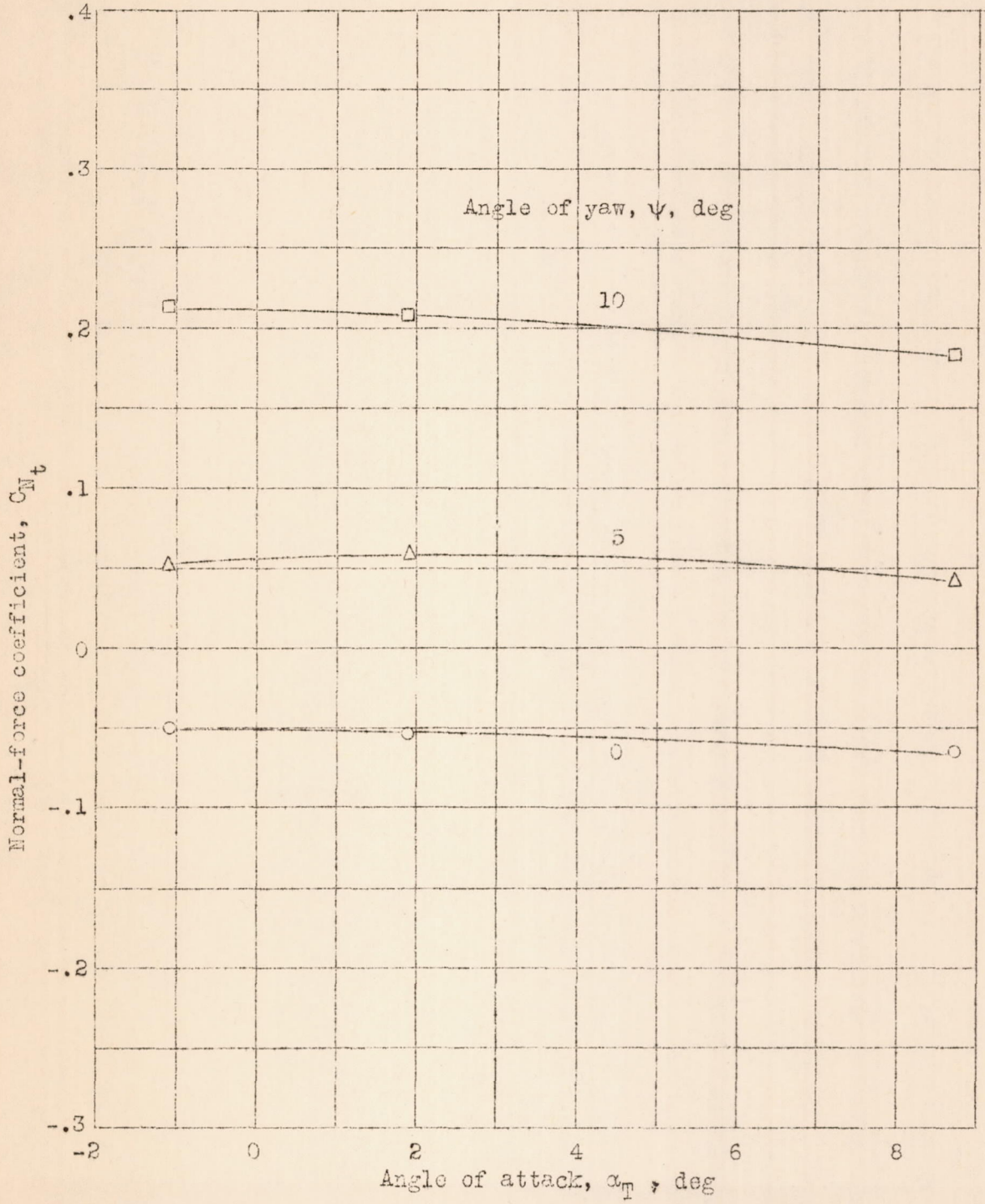

Figure 16.- Variation of vertical-tail normal-force coefficient with angle of attack. Propeller removed.

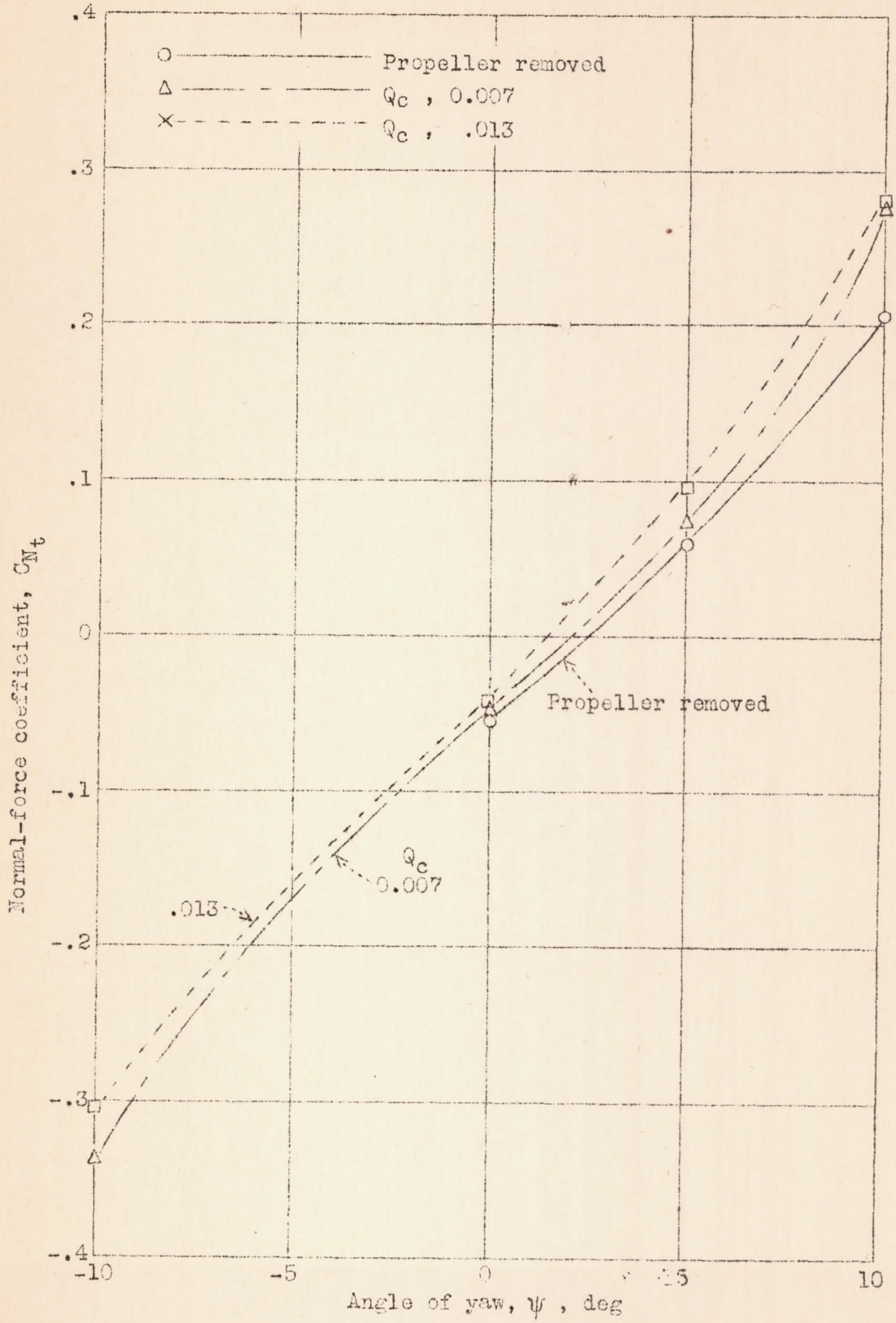

Figure 17.- Effect of propeller operation on the variation of vertical-tail normal-force coefficient with angle of yaw. C_L, 0.294.

L-426

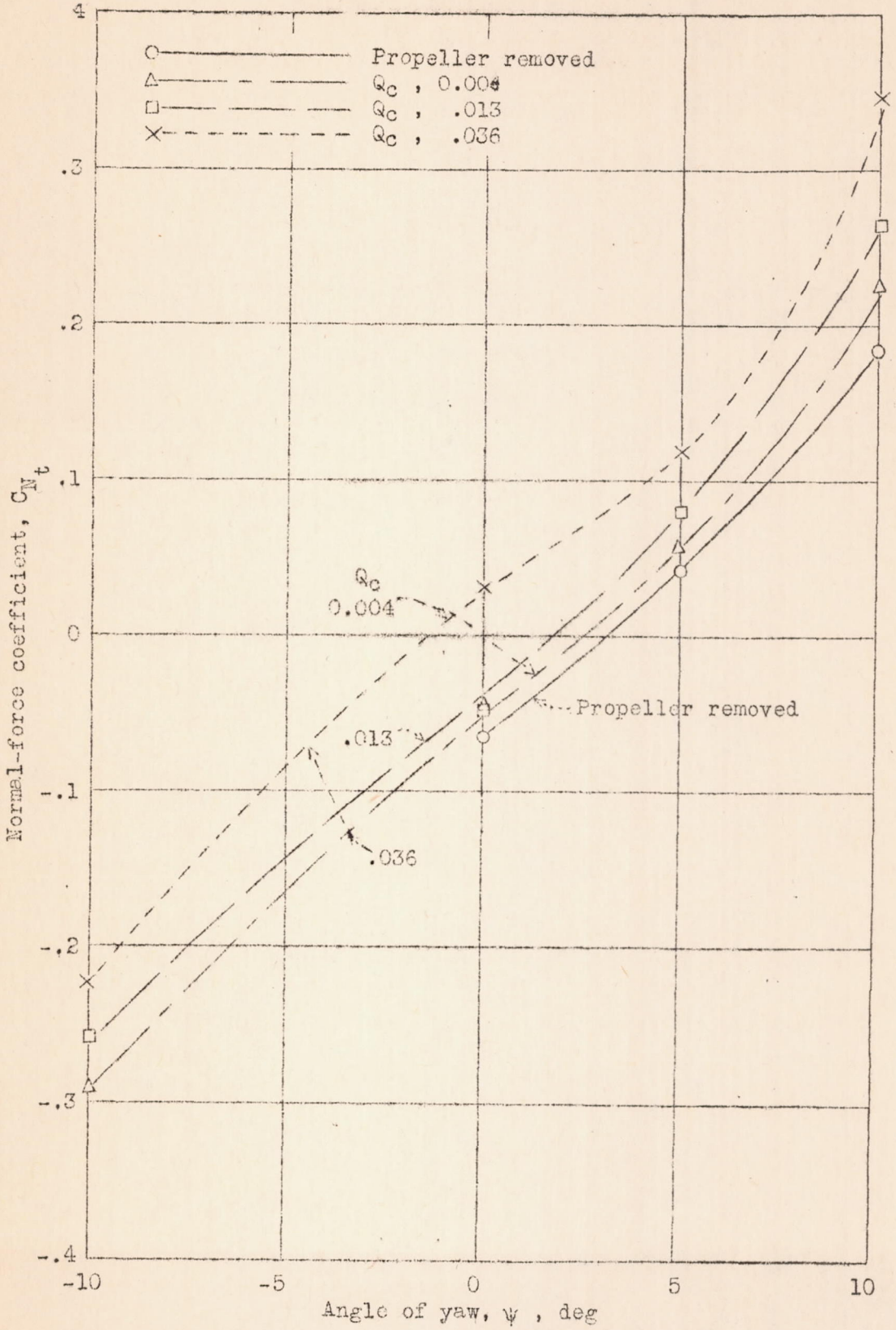

Figure 18.- Effect of propeller operation on the variation of vertical-tail normal-force coefficient with angle of yaw. C_T , 0.820.

L-426

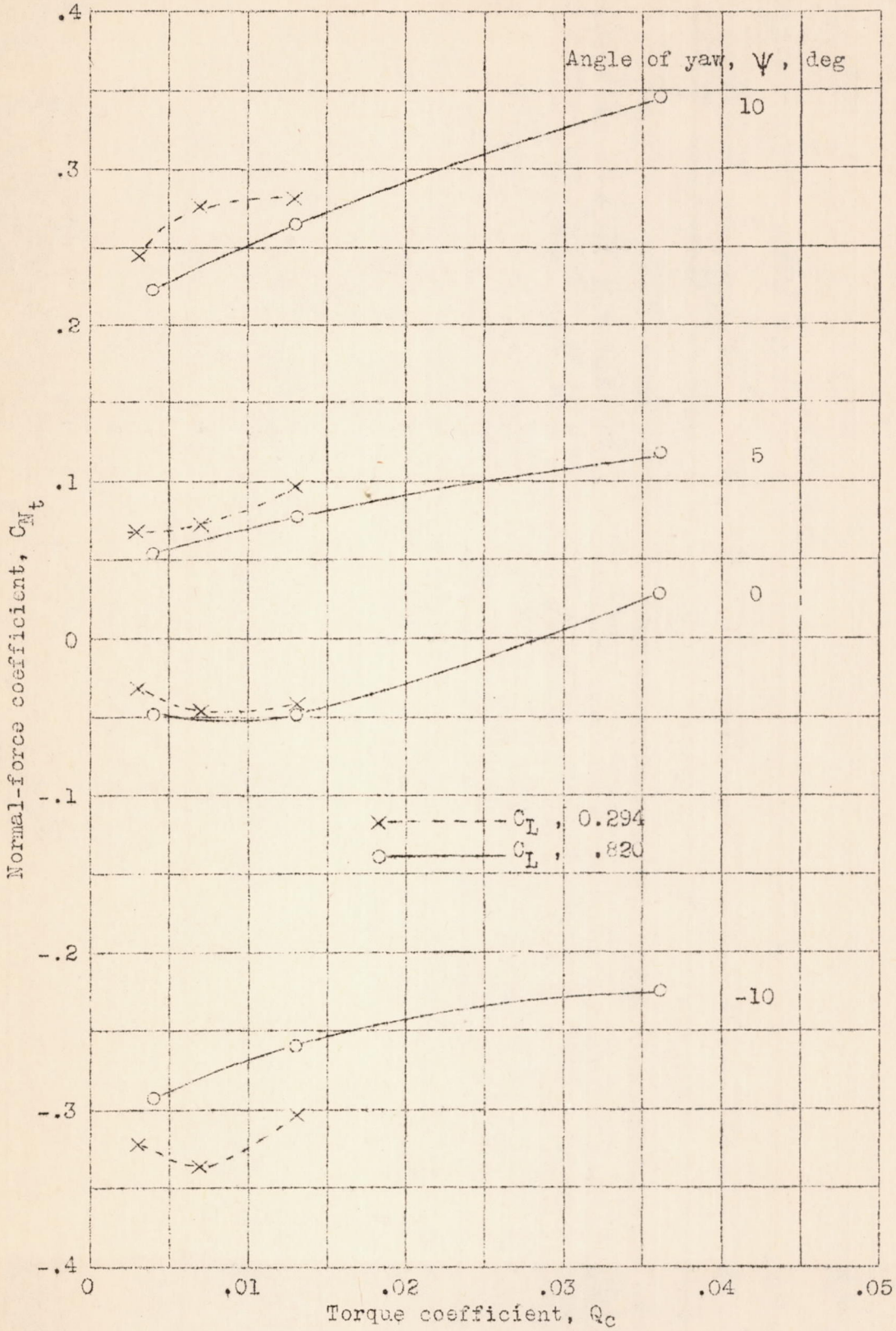

Figure 19.- Effect of slipstream rotation on the vertical-tail normal-force coefficient.